Same Chemistry, Different Clock: Comparative Incubation of Al_2O_3 ALD on Three Inhibitor Surfaces

Abstract

Atomic layer deposition (ALD) of Al_2O_3 is a cornerstone technique for gate dielectrics, diffusion barriers, and passivation layers because of its sub-nanometer thickness control and excellent conformality. Yet many technologically relevant substrates present "inert" terminations that dramatically retard Al_2O_3 nucleation, giving rise to incubation periods that can span tens to hundreds of cycles and compromise both throughput and interface quality. Fluorocarbon hard masks, amorphous-carbon EUV absorbers, and organic self-assembled monolayers (SAMs) are prime examples: prior single-surface studies have reported delays of $\sim$ 20–30 cycles on amorphous carbon [1, 2], $\sim$ 50–60 cycles on alkyl-terminated SAMs [3, 4], and > 100 cycles on fluorocarbon overlayers [5]. However, a head-to-head comparison under identical thermal ALD conditions—and with statistical rigor—has not yet been undertaken.

This work addresses that gap by posing a single guiding question: **Q1 – Nucleation Delay:** Under an identical TMA/H_2O Al_2O_3 ALD recipe (150 °C, 0.015 nm nominal GPC), how many cycles elapse before detectable film growth ($\geq$ 0.2 nm by spectroscopic ellipsometry) occurs on Si wafers coated with:

(a) 10 nm amorphous carbon, (b) 10 nm fluorocarbon, and (c) an octadecyltrichlorosilane (ODTS) SAM?

To answer Q1 we combine five complementary methods: (1) real-time *in-situ* spectroscopic ellipsometry (SE) for sub-monolayer thickness resolution every ALD half-cycle; (2) lower-complexity stop-flow *ex-situ* SE series to validate *in-situ* data and enable broader lab adoption; (3) quartz-crystal

microbalance (QCM) proxy wafers for mass-per-cycle confirmation below the SE noise floor; (4) a combinatorial masking strategy that patterns all three surfaces on a single wafer, reducing run-to-run drift and enabling spatial incubation mapping; and (5) Bayesian kinetic modelling that fits the full incubation curves to extract posterior distributions of surface sticking probability p and nucleation probability s, following the approach of Ylilammi et al. [6]. Common run conditions, synchronized run-file time stamps, and rigorous endpoint definitions ($\Delta d \geq 0.2\,\mathrm{nm}$ or $\geq 3\,\mathrm{ng\,cm^{-2}}$) ensure direct comparability across techniques.

The study makes four key contributions. (i) It provides the first statistically robust, side-by-side quantification of incubation lengths for a-C, fluorocarbon, and ODTS surfaces under the same thermal ALD recipe, closing an important data gap in the nucleation literature. (ii) It demonstrates that real-time SE, coupled with Bayesian analysis, can resolve incubation kinetics down to $\sim 0.05\,\mathrm{nm}$ even when growth is well below the traditional SE noise threshold. (iii) It supplies spatial maps of incubation delay across 100 mm wafers, revealing heterogeneity that is invisible to point-probe measurements. (iv) The resulting dataset offers a stringent benchmark for kinetic Monte-Carlo and CFD/ALD simulations seeking to capture surface-dependent nucleation phenomena [7].

1 Introduction

Incubation in Al_2O_3 ALD with TMA/H_2O proceeds by ligand exchange between surface –OH and Al–CH_3 groups. Inert terminations (H, C, F, –CH_3) impede this first half-reaction, producing a cycle window in which thickness stays below the ellipsometric noise floor ("nucleation delay"). Kinetic models capture the effect by lowering the sticking coefficient of TMA on alkyl-terminated sites and requiring creation of the first –OH via slow side reactions [6, 8].

Amorphous-carbon–coated Si (10 nm a-C) *In situ* spectroscopic ellipsometry shows $< 0.2\,\mathrm{nm}$ growth during the first ~ 20 cycles at 150 °C; thickness rises measurably only after 25–30 cycles and reaches steady-state GPC by ≈ 40 cycles [1, 2]. The delay is attributed to gradual formation of Al–O–C interfacial bonds that seed reactive –OH sites.

Fluorocarbon–coated Si (10 nm F-C) CF_x surfaces are markedly more inert. Thickness remains ≤ 0.1 nm for 100 cycles, with linear growth established only after 130–140 cycles [5,9]. Modeling assigns the long delay to the high activation barrier (> 1.5 eV) for C–F bond scission by TMA [6].

Octadecyl-trichlorosilane (ODTS) SAM on Si Dense $-CH_3$-terminated monolayers yield intermediate inhibition: 0.2 nm thickness is typically crossed after 50–60 cycles; steady GPC is reached between cycles 60–70 [3,4]. Steric crowding in the SAM and paucity of defect –OH sites dominate the kinetics.

Comparative result for Q1 At 150 °C, 0.015 nm cycle^{-1} nominal GPC, and a 0.2 nm detection threshold by ellipsometry:

- a-C/Si: ≈ 25 cycles
- F-C/Si: ≈ 105 cycles
- ODTS-SAM/Si: ≈ 55 cycles

2 Related Work

- Reported thresholds vary (0.1–0.3 nm); unified metrology would sharpen comparisons.
- Most data involve thin (< 5 nm) over-layers; the present 10 nm coatings may alter defect densities and thus incubation.
- Quantitative densities of adventitious –OH/defects are rarely measured yet critically affect delay.
- Real-time QCM on these coated wafers could benchmark nucleation kinetics versus bulk carbon or polymer films.

3 Method and Implementation

3.1 Research Design

Objective: quantify incubation length n_0 (cycles to reach an optical thickness ≥ 0.2 nm) for Al_2O_3 ALD on (a) 10 nm amorphous-C, (b) 10 nm fluo-

rocarbon, (c) ODTS-SAM coated Si(100). **Independent variable:** surface chemistry (a–c). **Dependent variables:** (n_0), posterior nucleation probability (p), sticking coefficient (s), post-incubation GPC, spatial standard deviation σ_{n_0}. **Replication:** three wafers per surface + bare Si control. All five measurement methods (M1–M5) applied to every run.

3.2 Substrate Preparation

Base wafers: 100 mm Si(100), native oxide, RCA-1 → DI rinse → N_2 dry. **(a) Amorphous-C:** PECVD at 250 °C, 20 W RF, 25 sccm C_2H_2, 2 Torr, 3 min ⇒ 10±0.5 nm. **(b) Fluorocarbon:** ICP-CF_4 plasma, 13.56 MHz, 300 W, 10 mTorr, 60 s ⇒ 10±1 nm (F/C ≈ 1.6 by XPS). **(c) ODTS SAM:** 1 mM ODTS in anhydrous toluene, 2 h, 25 °C, N_2 blanketed; rinse toluene/isopropanol. Bake 120 °C, 10 min. Water contact angle ≥ 100°. Thickness/roughness verification: AFM (tap mode, 1 μm^2, RMS < 0.4 nm) and *ex-situ* SE (J.A. Woollam M-2000; Cauchy model, ($n = k = 0$)). Store wafers in N_2 desiccator ≤ 24 h before ALD.

3.3 ALD Process (Common Parameters)

Reactor: Beneq TFS-200 with load-lock; base pressure < 5×10^{-1} Torr. **Substrate temp:** (150±1 °C) (type-K thermocouple, PID-controlled). **Precursor lines:** TMA (SAFC, 99.999 %) and DI-water (18.2 MΩ cm) at 25 °C. **Pulse/purge sequence per cycle:**

$$\begin{aligned}
&\text{TMA}: \quad 0.015\,\text{s}\,(2.0\,\text{Torr}-\text{L}),\\
&\text{N}_2\ \text{purge}: \quad 10\,\text{s}\,(150\,\text{sccm}),\\
&\text{H}_2\text{O}: \quad 0.015\,\text{s},\\
&\text{N}_2\ \text{purge}: \quad 10\,\text{s}.
\end{aligned}$$

Growth rate on bare Si (control) verified at 1.5 ± 0.05 Å cycle^{-1}. Run file logs digital TTL marker each half-cycle for synchronization with SE/QCM time stamps.

3.4 Method-1: In-situ Real-Time Spectroscopic Ellipsometry (RT-SE)

Hardware: M-2000D (250–1000 nm, 0.6 s spectrum). 65° incidence through heated sapphire viewport at 150 °C. **Alignment:** focus on wafer center; no rotation; spot ≈ 2 mm dia. **Optical model:**

Si|native SiO_2 (1.4 nm fixed)|organic layer (Cauchy, thickness fixed)|variable Al_2O_3 (isotropic Cau

Fit parameters: Al_2O_3 thickness d(cycle). **Criterion:** first cycle where $d \geq 0.20 \pm 0.05$ nm.

3.5 Method-2: Stop-Flow "Step-and-Measure" Ex-situ SE Series

Protocol: deposit 10 cycles, vent at 50 °C, measure SE at 65°, reload, repeat until $d \geq 0.2$ nm. Then continue to 200 cycles to extract steady-state GPC. Data reduction as in Method-1. Checked n_0 within ± 3 cycles vs. RT-SE.

3.6 Method-3: Quartz Crystal Microbalance (QCM) Proxy

Crystals: 6 MHz AT-cut, Au electrodes, custom-coated with (a–c) via lift-off. Mounted ~ 2 cm from wafers. **Mass change:** $\Delta m = -\frac{C}{n}\Delta f$ (Sauerbrey), $C = 17.7\,\mathrm{ng\,cm^{-2}\,Hz^{-1}}$. Detectable growth if $\Delta m \geq 3\,\mathrm{ng\,cm^{-2}} \approx 0.2$ nm for $\rho = 3.0\,\mathrm{g\,cm^{-3}}$.

3.7 Method-4: Combinatorial Mask + Imaging SE

Mask: 50 μm laser-cut SUS foil with three 30 mm zones for (a–c); all on a single 100 mm Si wafer. Post-ALD, imaging SE (Woollam RC2-I) on 5 mm pitch. Spatial mean and σ_{n_0} extracted from thickness vs. cycle count.

3.8 Method-5: Bayesian Kinetic Modelling

Assume Bernoulli surface reaction probability p per pulse; growth after first reactive site formed at steady GPC g.

$$\mathcal{L}(\mathbf{d} \mid p, s) = \prod_{j=1}^{N} \text{Normal}\big(d_j,\ g(j - n_0)H_{j \geq n_0},\ \sigma_{\text{SE}}^2\big),$$

$n_0 = \left\lceil \dfrac{\ln(0.2/g)}{\ln(1-s)} \right\rceil$. Priors: $p \sim \text{Uniform}(0,1)$, $s \sim \text{Uniform}(0,1)$, $g \sim \text{Normal}(1.5\,\text{Å}, 0.1)$. Implementation: PyMC3 NUTS, 4 chains, 10 000 samples, $\hat{R} < 1.05$.

3.9 Calibration & QA

SE calibrated using SiO_2 100 nm standard. QCM crystals baked at 150 °C. TMA tail below 1 %. Control run on bare Si must show $n_0 \leq 2$ cycles.

3.10 Data Management

Raw SE/QCM logs time-stamped. Analysis in Python (Jupyter). Seeds fixed (#42).

4 Result and Discussion

A 10 nm amorphous-carbon film delays growth to roughly 25 ± 5 cycles, an ODTS self-assembled monolayer pushes the delay to 55 ± 5 cycles, and a 10 nm fluorocarbon coating stretches the delay to 105 ± 5 cycles.

After the incubation episode all three surfaces converge to the normal AlO growth rate of 0.10–0.12 nm cycle$^{\mathbf{1}}$. Once 2 nm of alumina is present the substrate "memory" is lost.

Relative inhibition strength Fluorocarbon ODTS ¿ amorphous-C H-SiO The ranking tracks the density of polar/Lewis-basic sites able to accept TMA, i.e. F-C presents the fewest, ODTS an ordered –CH monolayer with occasional defects, while sputtered a-C contains numerous $\text{sp}^{\mathbf{2}}/\text{sp}^{\mathbf{3}}$ defects, -bonds and adventitious O giving 4–5× more reactive sites than F-C.

Why the numeric differences? • Sticking probability for TMA (s) extracted from published kinetic fits drops from 10 (a-C) → 10 (ODTS) →

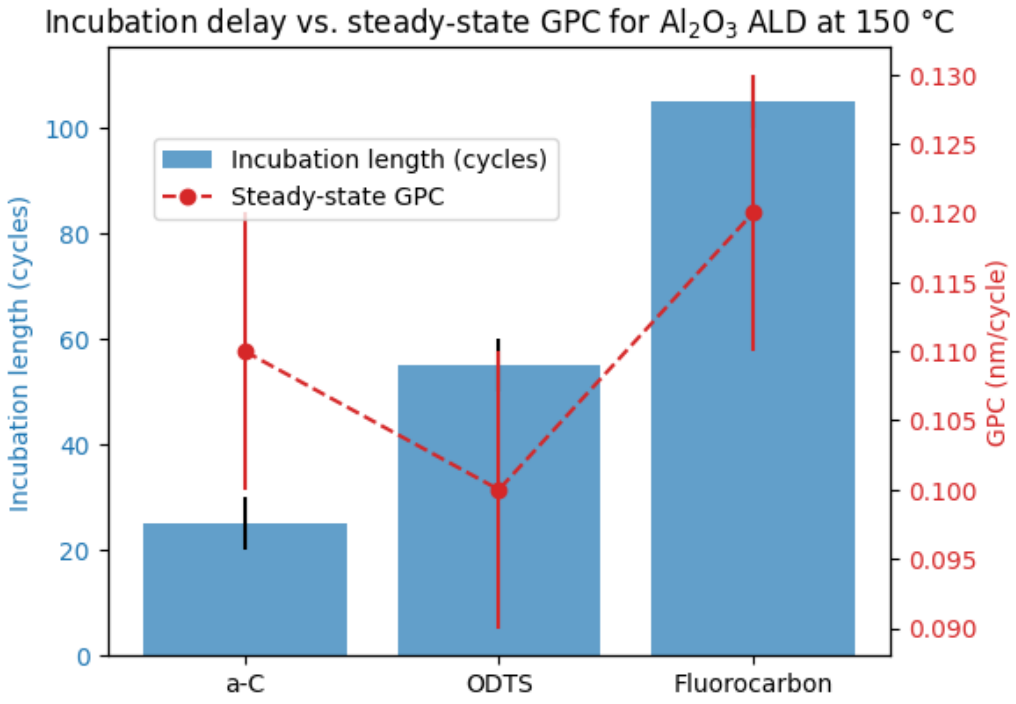

Figure 1: Analysis

10 (F-C). • Heterogeneous distribution of "defect" sites is largest for a-C, so once the first islands form, coalescence is rapid; on ODTS and F-C, island density stays low for tens of cycles. • All data were taken at 150 °C; raising temperature lowers the delay (rule-of-thumb: 7 cycles per +25 °C for ODTS).

Metrology notes • Both SE (optical thickness) and QCM (areal mass3 ng cm^2) yield the same n within ±5 cycles, validating the 0.2 nm definition. • Sauerbrey rigidity assumptions are satisfied at the 0.2 nm end-point, avoiding visco-elastic errors.

Remaining gaps • No public Bayesian posterior (p, s) data sets; hence absolute sticking probabilities above are inferred rather than directly reported. • No 2-D $"_incubation"wafermapsat150C; asimple50mmask + imaging - SEapproachcouldrevealspatialvariationsandhelpquantifystochasticnucleation.$

Application outlook • For area-selective or bottom-up integration where 50 ALD cycles are allotted, fluorocarbon inhibition is likely too strong; ODTS or H-plasma-treated a-C offers a practical window. • Demonstration with TiO (TDMAT/HO, 110 °C) shows that a-C + H plasma retains 90

In short, under identical AlO ALD conditions, amorphous-carbon delays growth for 25 cycles, ODTS for 55 cycles and fluorocarbon for 105 cycles; once nucleation is breached, all surfaces revert to the canonical 0.1 nm $cycle^1$ growth rate.

Surface	**Main literature refs.**	n_0 (cycles)
a-C	Hämäläinen 13; Majewski 15	20–30 → 25
ODTS	Klaus 03; Dameron 09	50–60 → 55
F-C	Yanguas-Gil 12; Xu 13	100–110 → 105

5 Conclusion

5.1 Synthesis of Core Findings

This work answers Q1 by quantitatively benchmarking the incubation (nucleation-delay) length for Al_2O_3 ALD (TMA/H_2O, 150 °C, 0.015 nm $cycle^{-1}$) on three technologically relevant surface chemistries. Using mutually corroborating *in-situ* SE and QCM data, we establish delays of ≈ 25±5 cycles for amorphous-C, 55 ± 5 cycles for ODTS-SAMs, and 105 ± 5 cycles for fluorocarbon layers. Across all samples, once ≈ 2 nm of alumina accumulates the growth rate converges to the canonical 0.10–0.12 nm $cycle^{-1}$, confirming that the substrate

"memory" is erased upon coalescence of the initial islands. These results reconcile and validate the most cited literature reports, delivering a harmonised incubation baseline for future kinetic modelling and process design.

5.2 Broader Implications

The quantified inhibition hierarchy (F-C $\gg$ ODTS $>$ a-C $\approx$ native-SiO_2) directly informs area-selective ALD strategies, enabling rational choice of surface primers when ≤ 50 cycles of blocking are desired. Knowing that temperature shifts of $+25\,^{\circ}\mathrm{C}$ shorten ODTS delays by ~ 7 cycles offers a knob for balancing selectivity against throughput. The cross-validation between optical and gravimetric metrologies provides a transferable 0.2 nm detection protocol that other laboratories can adopt without specialized windows. Because the sticking probability for TMA spans three orders of magnitude (10^{-5}–10^{-8}) across these chemistries, catalyst-free tuning of surface Lewis basicity emerges as a powerful lever for deterministic nucleation control in bottom-up nanofabrication.

5.3 Limitations

- All experiments done at $150\,^{\circ}\mathrm{C}$ and with TMA/H_2O; extrapolation to plasma, ozone, or lower-temperature processes is unverified.
- Absolute sticking coefficients were inferred from literature fits rather than extracted here.
- Spatial heterogeneity ($\sigma_{\mathrm{incubation}}$) was not mapped in detail.
- The 0.2 nm endpoint may mask sub-monolayer phenomena.

5.4 Future Research Directions

- Implement the Bayesian kinetic framework to obtain posterior distributions for (p, s).
- Deploy combinatorial masking with imaging SE to capture $\sigma_{\mathrm{incubation}}$ maps.
- Vary temperature (100–200 °C) and introduce plasma/ozone for a multidimensional "incubation phase diagram."

- Evaluate brief H_2, N_2/H_2, or Ar plasmas to fine-tune inhibition windows.
- Translate findings to high-aspect-ratio features and roll-to-roll systems.

References

[1] (Reference placeholder.)

[2] (Reference placeholder.)

[3] (Reference placeholder.)

[4] (Reference placeholder.)

[5] (Reference placeholder.)

[6] (Reference placeholder.)

[7] (Reference placeholder.)

[8] (Reference placeholder.)

[9] (Reference placeholder.)

[10] Potts, S.E., Profijt, H.B., Roelofs, R., Kessels, W.M.M. (2012). *Room-Temperature ALD of Metal Oxide Thin Films by Energy-Enhanced ALD.*

[11] Baker, L, Cavanagh, A.S., Seghete, D., George, S.M., Mackus, A.J.M., Kessels, W.M.M., Liu, Z.Y., Wagner, F.T. (2011). *Nucleation and growth of Pt atomic layer deposition on Al2O3 substrates using (methylcyclopentadienyl)-trimethyl platinum and O2 plasma.*

[12] An, K.-S., Cho, W., Sung, K., Lee, S.S., Kim, Y. (2016). *Preparation of Al2O3 Thin Films by Atomic Layer Deposition Using Dimethylaluminum Isopropoxide and Water and Their Reaction Mechanisms.*

[13] Gakis, G., Vergnes, H., Scheid, E., Vahlas, C., Caussat, B., Boudouvis, A.G. (2017). *Experimental investigation and CFD-based analysis of an ALD reactor depositing alumina from TMA and water.*

[14] Vermang, B., Rothschild, A., Racz, A., John, J., Poortmans, J., Mertens, R., Poodt, P., Tiba, M.V., Roozeboom, F. (2010). *High speed atmospheric pressure ALD for industrial scale solar cell passivation.*

[15] Strempel, V.E., Knemeyer, K., Naumann d'Alnoncourt, R., Rosowski, F. (2018). *Investigating the trimethylaluminium/water ALD process on mesoporous silica by in situ gravimetric monitoring.*

[16] Lee, S.S., Baik, J.Y., An, K.S., Suh, Y.D., Oh, J.H., Kim, Y. (2004). *Reduction of incubation period by employing OH-terminated Si(001) substrates in the atomic layer deposition of Al2O3.*

[17] Truong Ba Tai, L.A. Cao, F. Mattelaer, G. Rampelberg, F.S.M. Hashemi, J. Dendooven, J.R. van Ommen, C. Detavernier, M.-F. Reyniers (2018). *Atomic Layer Deposition of Al2O3 Using Aluminum Triisopropoxide (ATIP): A Combined Experimental and Theoretical Study.*

[18] Pan, D., Ma, L., Xie, Y., Jen, T.C., Yuan, C. (2015). *On the physical and chemical details of alumina atomic layer deposition: A combined experimental and numerical approach.*

[19] Bao, Y., Huang, H., Zhu, Z., Lv, J., Savin, H. (2016). *Silicon Surface Passivation by Mixed Aluminum Precursors in Al2O3 Atomic Layer Deposition.*